Journal of Materials Chemistry A

ROYAL SOCIETY OF CHEMISTRY

PAPER

View Article Online
View Journal

Cite this: DOI: 10.1039/d5ta10296k

Mechanistic insights into defect-governed ion migration and phase instability in mixed-halide perovskites

Yueran Xiang, [a] Haimeng Xin,[a] Chenyu Wang,[a] Fuyi Zhou, [a] Hengyu Zhang,[a] Pengjie Hang,[a] Lingbo Xu, [b] Xuegong Yu, [a] Jingjing Xue,[a] Deren Yang [a] and Zhenyi Ni*[ac]

Ion migration critically underpins the operational instability of metal halide perovskites, yet the fundamental mechanisms by which defect chemistry and physics govern ion migration in mixed-halide perovskites, and their critical role in driving the distinct instability pathways under dark *versus* illuminated conditions, remain inadequately understood. Here, we investigate ion-migration dynamics coupled with defect and phase segregation in $FAPb(I_{1-x}Br_x)_3$, uncovering a defect-governed evolution of ion migration across different Br compositions. Under dark conditions, ion migration is revealed to be dominated by the specific characteristics of halide interstitial defects, whereas illumination triggers FA-cation migration that strongly correlates with the deep-level defect density. Despite exhibiting comparable halide-migration barriers, high-Br compositions undergo a two-state phase segregation process, comprising an initial thermodynamically driven halide separation followed by a kinetically accelerated regime facilitated by a substantial reduction in the halide migration barrier. These findings provide essential insights for stabilizing wide-bandgap perovskites in high-efficiency tandem photovoltaics.

Received 17th December 2025
Accepted 11th March 2026

DOI: 10.1039/d5ta10296k

rsc.li/materials-a

Introduction

Metal halide perovskites (MHPs) have emerged as one of the most promising classes of semiconductors for next-generation optoelectronic technologies, including solar cells,[1–3] light-emitting diodes,[4–6] and photon or radiation detectors.[7–9] Their rapid progress in device performance has firmly positioned MHPs as compelling candidates for low-cost, high-efficiency optoelectronics.[10–13] Nevertheless, long-term operational stability remains the key unresolved obstacle to their practical deployment and commercialization.[14–17] Among the various degradation pathways, ion migration which is rooted in the inherently soft lattice and ionic bonding framework of MHPs and intricately coupled to their composition, structure, and defect dynamics stands as a persistent and fundamental challenge underlying their instability.[18–20] This intrinsic mechanism of instability cannot be eliminated by device encapsulation alone, underscoring the need for a deeper understanding and more effective materials-level stabilization strategies.

The investigation of ion migration in MHPs has therefore been a long-standing research focus, with early studies primarily seeking to identify the migrating ionic species and quantify basic migration parameters.[21–26] More recent efforts have shifted toward elucidating the dynamics of ion migration and its interplay with defect formation and structural evolution.[27–30] However, earlier studies have been mainly devoted to iodine-based perovskite compositions, whose insights cannot be straightforwardly extrapolated to the mixed-halide wide-bandgap systems that are critically important for high-efficiency perovskite-based tandem solar cells. To date, a few studies have tentatively examined ion-migration behavior in mixed-halide perovskite solar cells (PSCs), where bromide (Br) incorporation into methylammonium lead iodide ($MAPbI_3$) has been shown to exert distinctly different ion-migration dynamics.[28,29,31,32] Yet, the mechanistic role of Br incorporation in modulating ion-migration behavior, its coupling with the underlying defect chemistry and physics, and, importantly, its connection to the halide phase segregation that plagues wide-bandgap perovskites remain largely unresolved. This knowledge gap is particularly relevant for the currently most promising MA-free, FA-based compositions, as their ion migration behavior and the role of defects in driving halide segregation remain less studied and understood compared to their MA-containing counterparts. Addressing these unresolved questions is essential for uncovering the mechanisms that govern ion migration and the subsequent phase segregation in mixed-

[a]State Key Laboratory of Silicon and Advanced Semiconductor Materials, School of Materials Science and Engineering, Zhejiang Provincial Key Laboratory of Optoelectronic Functional Materials and Devices, Zhejiang University, Hangzhou, Zhejiang 310027, China. E-mail: zyni@zju.edu.cn

[b]Zhejiang Key Laboratory of Quantum State Control and Optical Field Manipulation, Department of Physics, Zhejiang Sci-Tech University, Hangzhou 310018, China

[c]Shangyu Institute of Semiconductor Materials, Shaoxing 312300, China

halide wide-bandgap PSCs, providing invaluable guidance for enhancing the operational stability of perovskite-based tandem solar cells.

In this work, we present systematic investigation of ion-migration dynamics in FA-based mixed-halide perovskites $FAPb(I_{1-x}Br_x)_3$ (x = 0–0.25), spanning the compositional range most widely used in both standard and wide-bandgap perovskite solar cells with state-of-the-art efficiencies. We establish a mechanistic framework that links ion-migration kinetics, defect chemistry, and photoinduced phase instability in mixed-halide perovskites, elucidating the nature of defects that govern ion migration. By correlating ion-migration behavior with real-time phase-segregation dynamics, we uncover a two-stage segregation mechanism in which early-stage phase separation is driven by thermodynamic relaxation of halide inhomogeneity, followed by a kinetically accelerated regime triggered by a substantially reduced halide-migration barrier. These insights provide a unified defect – ion migration – phase segregation framework that is essential for stabilizing wide-bandgap perovskites in high-efficiency tandem photovoltaics.

Results and discussion

To elucidate how Br incorporation influences ion migration in $FAPbI_3$, we first fabricated a series of p-i-n structured $FAPb(I_{1-x}Br_x)_3$ perovskite solar cells (PSCs) with nominal Br fractions (x) ranging from 0 to 0.25. The device performance and corresponding current density–voltage (J–V) curves are shown in Fig. S1 and 1a. Comprehensive characterization studies, such as XRD, SEM, EDS, and PL spectroscopy, were conducted to assess the basic properties of these perovskite films including morphology, composition, crystallinity, lattice parameters, and bandgap. The XRD results demonstrate that all the perovskite films retain the cubic crystal structure with good crystallinities (Fig. 1b). EDS analysis revealed that although the actual Br content was slightly higher than the nominal concentration in the precursor solution, it exhibited a linear dependence on the intended composition with the nominal values (Fig. 1d). Therefore, for consistency with literature conventions, the nominal x values derived from the precursor solution are used throughout this work to denote the $FAPb(I_{1-x}Br_x)_3$ compositions.

Fig. 1c shows the evolution of the lattice constant of $FAPb(I_{1-x}Br_x)_3$ extracted from XRD analysis (Fig. 1b) as a function of Br content. Overall, the lattice constant decreases nearly linearly with increasing Br concentration, except for the sample with $x = 0.025$, which exhibits a slight positive deviation from this linear trend. To elucidate the origin of this anomaly, we first extracted the bandgaps of $FAPb(I_{1-x}Br_x)_3$ from the PL spectra (Fig. 1e), which display an approximately linear increase with Br content (Fig. 1f). This linearity suggests that the fraction of Br atoms substituting for I in the halide lattice site which is responsible for bandgap widening is proportionate to the nominal Br composition, thereby excluding the possibility of incomplete Br substitution in the lattice site of halides as the cause of the anomalously large lattice constant observed for the $x = 0.025$ sample. Instead, we tentatively attribute this deviation to the formation of additional halide interstitial defects at low Br concentrations, as will be discussed later.

Then we performed transient ion drift (TID) measurement to evaluate the ion-migration behaviors in $FAPb(I_{1-x}Br_x)_3$ PSCs, as schematically shown in Fig. 2a and interpreted in Fig. S2–S4.

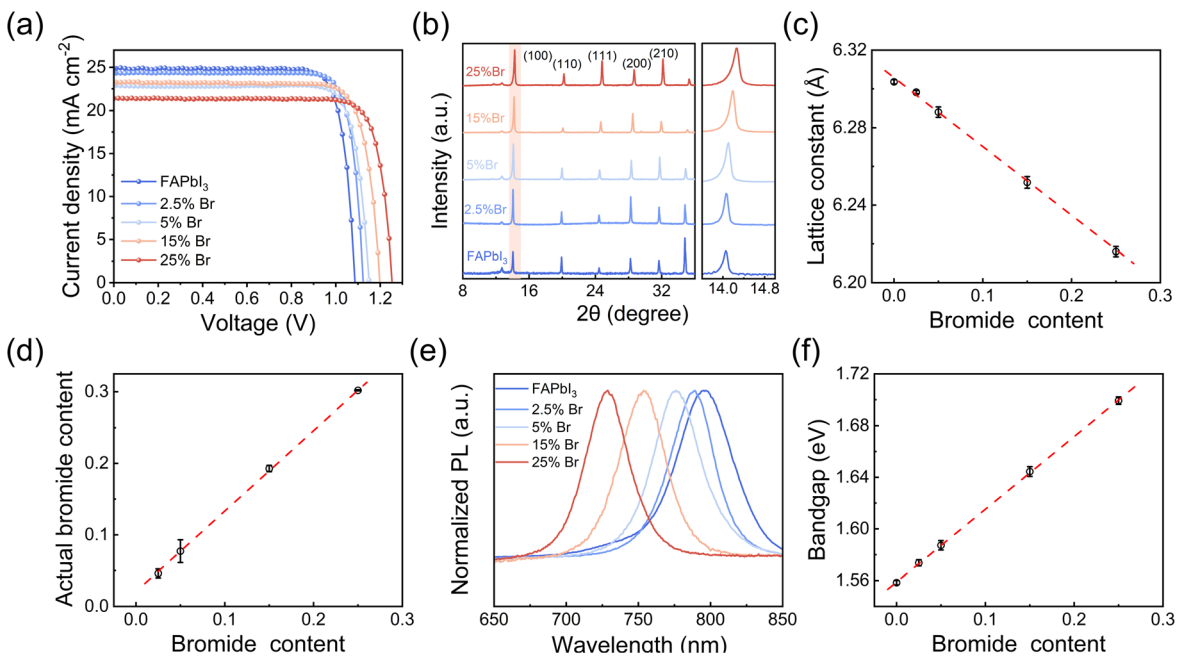

Fig. 1 Characterization of $FAPb(I_{1-x}Br_x)_3$ perovskite films with varying bromine content (x). (a) Current density–voltage (J–V) curves of the corresponding solar cells. (b) XRD patterns and (c) the derived lattice constant as a function of x. (d) Actual *versus* nominal bromine content. (e) PL spectra and (f) the corresponding optical bandgaps. The circles represent average values, with error bars denoting the standard deviation from five independent film tests.

The TID technique is employed to characterize ion migration in the perovskite layer by monitoring the temperature-dependent relaxation of capacitance after an applied voltage step. Capacitance measurements were conducted at 10 kHz, corresponding to the frequency-insensitive plateau region of the capacitance spectrum (Fig. S3), to ensure minimal interference from dielectric dispersion. A forward bias of 1 V was applied for 5 seconds to narrow the depletion region and induce redistribution of charge carriers within the originally depleted zone, resulting in a measurable modulation of the device capacitance. The dark TID results reveal an anion migration process, as evidenced by the negative capacitance change (ΔC) observed in the p-i-n structure over the temperature range of 300–200 K (Fig. S4). This signal has been typically attributed to halide ion migration in PSCs.[25] Fig. 2b summarizes the activation energy (E_a) of halide ion migration derived from the TID analysis (Fig. S5). Interestingly, E_a exhibits a sharp decrease from 0.131 to 0.074 eV upon the introduction of 2.5% Br ($x = 0.025$), followed by a gradual increase with further Br addition. Notably, the range of activation energies obtained from our TID measurements is consistent with values reported for halide migration in hybrid perovskites using other computational and experimental techniques (Table S1). This agreement not only supports the assignment of our measured signal specifically to anion migration but also indirectly validates the reliability and effectiveness of the TID method for probing ionic kinetics in this material system, whereas the calculated mobile-ion concentration shows an opposite dependence on Br content (Fig. 2c). These results suggest that the 2.5% Br composition is the most susceptible to halide ion migration, characterized by the lowest E_a and highest mobile-ion concentration. All parameters extracted from TID measurements for halide ion migration are summarized in Fig. 2d.

To identify the primary factor governing ion migration in our mixed-halide perovskites, we first examined the grain size of the films to assess whether grain boundaries dominate ion transport by providing additional migration pathways. SEM images reveal that the average grain size decreases with increasing Br concentration (Fig. S6 and 3a). This trend, however, cannot account for the observed increase in E_a as the Br content increases from 2.5% to 25%. To further decouple the influence of grain size, we fabricated large-grain films with 2.5% and 25% Br incorporation, having grain sizes comparable to that of the pure $FAPbI_3$ film (Fig. S6 and 3a). Interestingly, E_a slightly decreases as the grain size increases (Fig. 2a), implying that halide ion migration in mixed-halide perovskites is predominantly determined by the intrinsic properties of the grain interior rather than by grain-boundary density in this case.

Previous studies have suggested that a reduced lattice constant would impose a compressive strain that led to the suppression of ion migration.[33,34] This effect could partially account for the increase in E_a observed at high Br concentrations, while it could not fully explain the initial decrease in E_a when less than 5% Br is incorporated into $FAPbI_3$. We therefore speculate that variations in defects are primarily responsible for the observed evolution of ion-migration behavior. Although

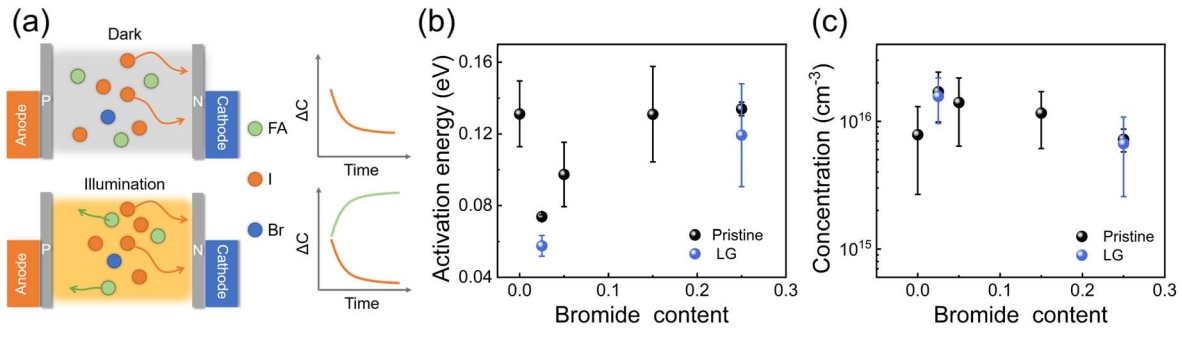

(d)

Composition	Activation energy (eV)	Diffusion coefficient at 300K ($cm^2 s^{-1}$)	Concentration (cm^{-3})
$FAPbI_3$	0.131 ± 0.021	$(2.258 \pm 1.299)\times10^{-8}$	$(1.379 \pm 1.403)\times10^{16}$
2.5% Br	0.074 ± 0.001	$(9.891 \pm 1.348)\times10^{-9}$	$(1.704 \pm 0.505)\times10^{16}$
	0.058 ± 0.001 (LG)	$(6.905 \pm 0.332)\times10^{-9}$ (LG)	$(1.570 \pm 0.430)\times10^{16}$ (LG)
5% Br	0.097 ± 0.020	$(1.707 \pm 0.570)\times10^{-8}$	$(1.407 \pm 0.820)\times10^{16}$
15% Br	0.131 ± 0.019	$(1.218 \pm 0.346)\times10^{-8}$	$(1.161 \pm 0.388)\times10^{16}$
25% Br	0.134 ± 0.003	$(5.131 \pm 0.822)\times10^{-9}$	$(7.223 \pm 1.037)\times10^{15}$
	0.119 ± 0.020 (LG)	$(3.074 \pm 1.020)\times10^{-9}$ (LG)	$(6.680 \pm 2.910)\times10^{15}$ (LG)

Fig. 2 Characteristics of mobile ions in $FAPb(I_{1-x}Br_x)_3$ perovskite solar cells *via* transient ion drift (TID) measurement. (a) Schematic illustration of the TID measurement principle in a p-i-n device structure. TID-derived (b) activation energy, (c) mobile ion concentration and (d) summary of the parameters for standard (pristine) and large-grain (LG) devices. Error bars represent the standard deviation from five independent device tests.

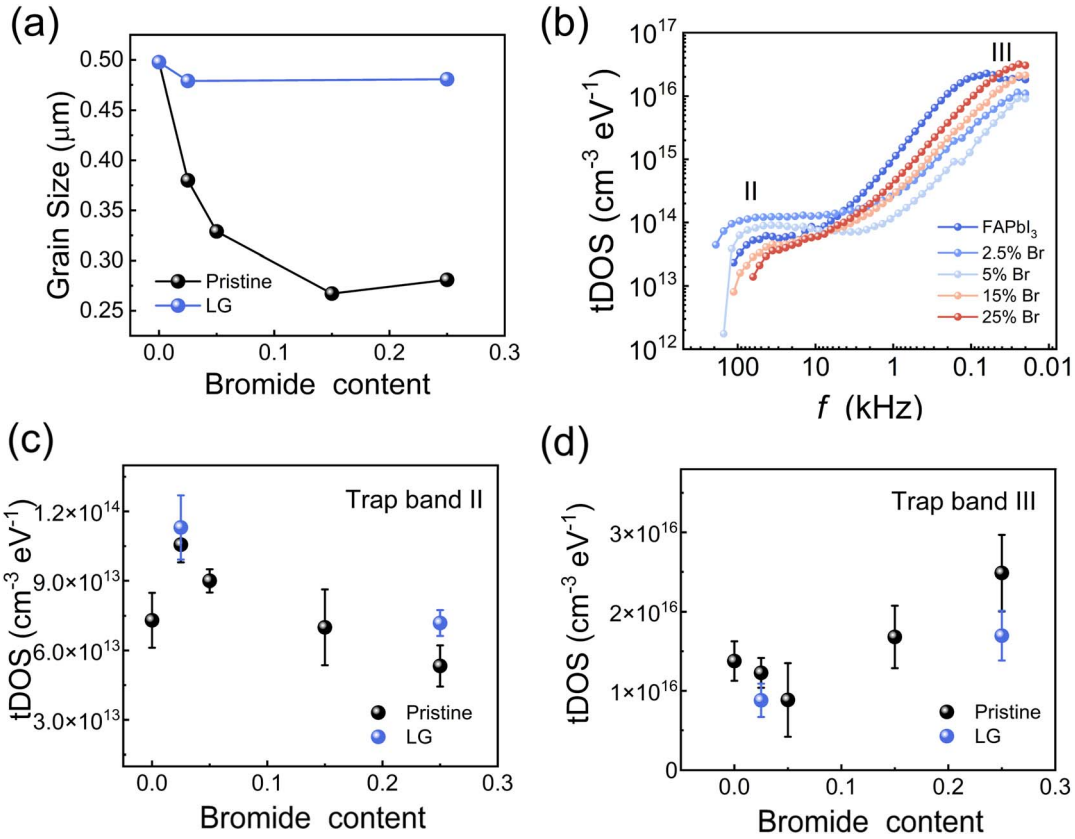

Fig. 3 Defect characterization of FAPb($I_{1-x}Br_x$)$_3$ films. (a) Grain size evolution with Br content for standard (pristine) and large-grain (LG) films. (b) Trap density of states (tDOS) spectra of corresponding solar cells, indicating trap bands II and III. Evolution of tDOS for (c) trap band II and (d) trap band III as a function of Br content (x). Error bars represent the standard deviation from five independent device tests.

such an awareness has been widely recognized for PSCs, a mechanistic understanding that directly links defect nature to ion migration and consequently the halide phase segregation has yet to be clearly established.

To this end, we performed thermal admittance spectroscopy (TAS) measurement on the FAPb($I_{1-x}Br_x$)$_3$ PSCs, as shown in Fig. 3b. The variations in the trap density of states (tDOS) for trap bands II and III as a function of Br concentration are summarized in Fig. 3c and d, respectively. Notably, the two trap bands exhibit contrasting trends with Br incorporation. Specifically, the tDOS of trap band II sharply increases upon introducing 2.5% Br and subsequently decreases with further Br addition, whereas trap band III initially decreases as the Br content increases from 0 to 5% and then increases again at higher Br concentrations. Intriguingly, the dependence of E_a and mobile halide-ion concentration on Br content in the dark closely mirrors the behavior of trap band II (Fig. 3c), *e.g.*, the 2.5% Br film exhibits the highest density of trap band II states, accompanied by the largest mobile-ion concentration and the lowest E_a. As our earlier work has identified iodine (halide) interstitial defects as the origin of trap band II in iodine-dominant perovskites,[35] we infer that halide-ion migration in FAPb($I_{1-x}Br_x$)$_3$ PSCs is primarily governed by halide interstitial defects. To further verify this correlation, we fabricated $FAPbI_3$ films with an additional 5% FAI, which markedly increased the trap density associated with iodine interstitials (Fig. S7a). As a result, the E_a for halide-ion migration decreased significantly from 0.131 eV to 0.063 eV (Fig. S7b), corroborating the correlation between trap band II and halide-ion migration dynamics. Besides, the elevated concentration of halide interstitials in the 2.5% Br sample would induce lattice expansion, thereby explaining the anomalously large lattice constant deviating from the linear trend (Fig. 1c).

Since the tDOS of trap band III shows no correlation with the variations of E_a and mobile-ion concentration with Br content under dark conditions, we tentatively ascribe this trap band to Pb- or FA-related defect states that remain largely immobile in the 300–200 K temperature range under dark conditions. To further understand ion-migration dynamics under the interplay of photo-generated carriers, we carried out TID measurements on the FAPb($I_{1-x}Br_x$)$_3$ PSCs under illumination, motivated by earlier studies reporting photo-induced A-site cation migration.[29,36]

Here, we found that upon illumination, both positive and negative ΔC signals were observed for all FAPb($I_{1-x}Br_x$)$_3$ PSCs except for the 2.5% Br sample (Fig. S8), indicating the coexistence of cation and anion migration in these perovskite films. However, while the transient polarity can serve as a qualitative indicator of the dominant migrating species at a given temperature, such assignments are not strictly unambiguous in

a multi-ionic system. The capacitance transients across the entire measured temperature range inevitably arise from the convolution of multiple ionic processes. The TID method monitors capacitance transients within a fixed experimental time window (milliseconds to seconds). Ionic contributions are observable only when their characteristic time constants (τ) fall within this window, such that ions with different mobilities selectively dominate the temperature-dependent transient capacitance response.[25,37,38]

To enable a tractable analysis, we adopt an approximate yet practical framework in which the rising edge of the transient capacitance is primarily attributed to cation migration, while the decaying edge is mainly associated with anion migration. This assignment allows a practical deconvolution of the coupled ionic contributions and enables the extraction of their respective activation energies (Fig. S9), which are further validated by a global fitting analysis (Fig. S10), as detailed in the SI. As Pb migration is energetically unfavorable[39] and no metallic Pb was observed after illumination under identical TID test conditions (Fig. S11),[40] we attribute the cation-migration component to FA^+, which is the sole A-site cation in our perovskite compositions. Fig. 4a summarizes the dependence of E_a for halide and FA^+ migration under illumination as a function of Br concentration. Notably, the E_a for halide migration under illumination follows a trend similar to that observed in the dark (Fig. 2b), whereas the E_a associated with FA^+ migration exhibits the opposite dependence on Br content. It first increases as the Br concentration increases to 5% and then decreases with further Br incorporation. This trend is surprisingly consistent with the Br-dependent evolution of the tDOS of trap band III, strongly suggesting that FA-related defect states are responsible for trap band III and that they govern the observed cation-migration behavior under illumination.

The non-monotonic evolution of FA-related defects likely arises from competing effects of halide substitution on local bonding and lattice strain, which together modulate the concentration of defect states contributing to trap band III.[41,42] It is noteworthy that the migration activation energy for FA^+ is significantly lower than that for halide anions under illumination, consistent with observations of MA^+ migration in $MAPbI_3$.[29] This reduction may be associated with interactions with photoexcited carriers or the influence of photoinduced lattice polarons,[43,44] although further investigation is required to elucidate the underlying mechanisms. It is interesting that we did not observe an appreciable cation-migration induced TID signal in the 2.5% Br PSCs under illumination. A plausible

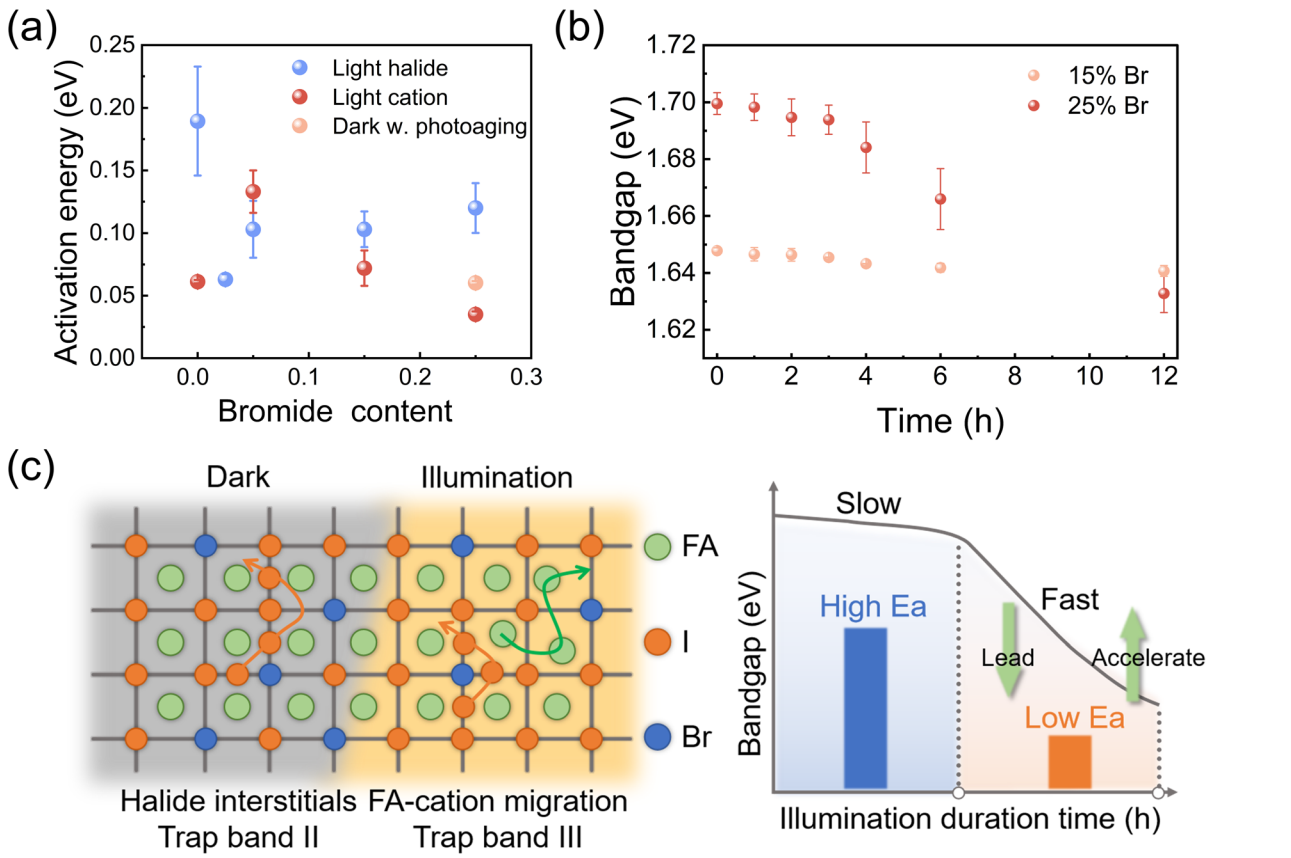

Fig. 4 Illumination-enhanced ion migration and photoinduced phase segregation in mixed-halide perovskites. (a) Activation energy for ion migration in $FAPb(I_{1-x}Br_x)_3$ solar cells under illumination (blue and red dots) and for photoaged devices in the dark (light orange dot). (b) Bandgap evolution of films with 15% Br and 25% Br during photo-aging. Error bars represent the standard deviation from five independent device tests. (c) Schematic diagrams for illustration of ion migration dynamics in the dark and under illumination for $FAPb(I_{1-x}Br_x)_3$ and the two-state phase segregation process for the high Br concentration component.

explanation is the elevated density of halide interstitial defects in this composition, which may effectively hinder or block the migration pathways available to A-site cations.

Finally, we discuss the correlation between ion-migration behavior and photoinduced phase segregation in mixed-halide PSCs with relatively high Br concentrations which are typically adopted for wide-bandgap PSCs. Fig. 4b shows the evolution of the bandgaps of the 15% and 25% Br perovskite films during photo-aging (carried out under identical conditions), extracted from the PL spectra in Fig. S12. It is seen that the 15% Br film exhibits no noticeable bandgap shift over 12 h of illumination, whereas the 25% Br film shows a clear bandgap reduction within the same period, indicating pronounced halide phase segregation at this composition. This stark contrast is consistent with the existence of a phase-segregation threshold above ~20% Br content, as first reported for $MAPb(Br_xI_{1-x})_3$.[43,45]

Given that the two films possess similar halide-migration activation energies and diffusion coefficients before phase segregation and exhibit similar macroscopic ion-transport properties (Fig. S13),[46] we infer that the initial phase segregation in the 25% Br film is primarily triggered by its thermodynamic instability associated with the initial halide inhomogeneity, rather than by ion-migration kinetics. This interpretation is supported by the relatively slow bandgap-narrowing observed during the first hour of illumination. After 1 h, however, the 25% Br sample exhibits a rapidly accelerated bandgap drop with continued photo-aging, suggesting that distinct mechanisms dominate the segregation process following the initial segregation stages. We further carried out dark TID measurement on the phase-segregated 25% Br PSCs after photoaging (Fig. S14), which revealed a significantly reduced activation energy for halide migration (Fig. 4a). This result indicates that once initial phase segregation occurs, enhanced halide migration could further amplify the phase segregation process and drives rapid bandgap narrowing. Collectively, these results demonstrate that halide phase segregation in mixed-halide wide-bandgap perovskites is governed by a synergy between thermodynamic instability and ion-migration kinetics, where the former initiates photoinduced phase separation and the latter is coupled with and accelerates subsequent segregation. Our findings highlight the necessity of simultaneously minimizing initial halide inhomogeneity and suppressing halide migration by increasing migration barriers to achieve highly phase-stable wide-bandgap PSCs.

Conclusions

In summary, this work establishes a mechanistic framework that directly links ion-migration kinetics, defect chemistry and physics with photoinduced phase instability in FA-based mixed-halide perovskites. By systematically resolving the roles of halide and cation migration across a wide Br compositional range, we reveal that ion migration in the dark is predominantly governed by halide interstitial defects, while under illumination FA-cation migration emerges, with its kinetics strongly correlated with deep defect states associated with trap band III, highlighting the defect-specific nature of ion transport in mixed-halide perovskites. The synergy between thermodynamic driving forces and defect-mediated ion migration gives rise to a two-stage phase-segregation process in Br-rich wide-bandgap compositions, ultimately accounting for the pronounced phase instability of high-Br perovskites.

Author contributions

Z. Ni conceived the project. Y. Xiang and Z. Ni designed the methodology and developed the theoretical framework. Y. Xiang, H. Xin, F. Zhou, and H. Zhang performed the experiments and collected the data. Y. Xiang and C. Wang conducted data analysis and figure visualization. P. Hang, L. Xu, X. Yu, J. Xue and D. Yang contributed to validation and provided critical resources. Z. Ni and Y. Xiang wrote the manuscript.

Conflicts of interest

There are no conflicts to declare.

Data availability

All data is available in the main text or the supplementary information (SI). The data supporting this article have been included as part of the SI. Supplementary information: experimental section including materials, device fabrication, and measurement; XRD, SEM, EDS and PL characterization of perovskite films; TID and TAS spectra of PSCs. See DOI: https://doi.org/10.1039/d5ta10296k.

Acknowledgements

This work was supported by the Baima Lake Laboratory Joint Fund of the Zhejiang Provincial Natural Science Foundation of China under Grant No. LBMHZ25F050001, the National Natural Science Foundation of China (No. 52303254 and 62474156) and Central Guidance Funds for Local Science and Technology Development Projects (2025ZY01012). The authors thank Dr Yangfan Lu (School of Materials Science and Engineering) for her help with XPS measurement and analysis.

Notes and references

1 Z. H. Wang, Z. Y. Han, X. B. Chu, H. T. Zhou, S. Q. Yu, Q. Zhang, Z. Xiong, Z. H. Qu, H. B. Tian, W. Wang, F. Wan, Y. B. Yuan, Y. Lin, Y. G. Yang, X. W. Zhang, Q. Jiang and J. B. You, *Adv. Mater.*, 2024, **36**, 2407681.
2 Q. Li, Y. C. Zheng, H. N. Wang, X. Y. Liu, M. Y. Lin, X. Y. Sui, X. S. Leng, D. Liu, Z. P. Wei, M. Y. Song, D. D. Li, H. G. Yang, S. Yang and Y. Hou, *Science*, 2025, **387**, 1069–1077.
3 Y. X. Lin, Z. C. Lin, S. L. Lv, Y. Shui, W. J. Zhu, Z. H. Zhang, W. H. Yang, J. B. Zhao, H. Gu, J. M. Xia, D. N. Wang, F. Q. Du, A. N. Zhu, J. Liu, H. R. Cai, B. Wang, N. Zhang, H. B. Wang, X. L. Liu, T. Liu, C. C. Kong, D. Zhou, S. Chen, Z. M. Yang, T. Li, W. Ma, G. J. Fang, L. Echegoyen, G. C. Xing,

S. C. Yang, T. Yang, W. T. Cai, M. Li, W. Huang and C. Liang, *Nature*, 2025, **642**, 78–84.
4 X. K. Liu, W. D. Xu, S. Bai, Y. Z. Jin, J. P. Wang, R. H. Friend and F. Gao, *Nat. Mater.*, 2021, **20**, 10–21.
5 L. M. Kong, Y. Q. Sun, B. Zhao, K. Y. Ji, J. Feng, J. C. Dong, Y. Z. Wang, Z. R. Liu, S. Maqbool, Y. G. Li, Y. G. Yang, L. J. Dai, W. Lee, C. Cho, S. D. Stranks, R. H. Friend, N. Wang, N. C. Greenham and X. Y. Yang, *Nature*, 2024, **631**, 73–79.
6 K. Y. Wei, T. Zhou, Y. Z. Jiang, C. J. Sun, Y. L. Liu, S. S. Li, S. Y. Liu, X. L. Fu, C. J. Hu, S. Tian, Y. G. Yang, X. W. Fu, N. Almasoud, S. M. H. Qaid, M. K. Nazeeruddin, H. Y. Hsu, W. D. Li, J. T. Kim, R. Long, W. Zhang, J. Chen and M. J. Yuan, *Nature*, 2025, **638**, 949–956.
7 Y. Zhou, C. B. Fei, M. A. Uddin, L. Zhao, Z. Y. Ni and J. S. Huang, *Nature*, 2023, **616**, 712–718.
8 H. M. Qin, B. Xiao, X. C. He, X. Ouyang, T. T. Gao, Y. Q. Wang, L. Y. Wang, Q. H. Sun, N. N. Shen, X. P. Ouyang and Y. H. He, *Nat. Commun.*, 2025, **16**, 158.
9 Z. Lin, L. Li, Y. Xu, D. Yang and Z. Ni, *Inf. Funct. Mater.*, 2025, **2**, 40–61.
10 L. N. Quan, B. P. Rand, R. H. Friend, S. G. Mhaisalkar, T. W. Lee and E. H. Sargent, *Chem. Rev.*, 2019, **119**, 7444–7477.
11 J. Y. Kim, J. W. Lee, H. S. Jung, H. Shin and N. G. Park, *Chem. Rev.*, 2020, **120**, 7867–7918.
12 M. Heydarian, M. Heydarian, P. Schygulla, S. K. Reichmuth, A. J. Bett, J. Hohl-Ebinger, F. Schindler, M. Hermle, M. C. Schubert, P. S. C. Schulze, J. Borchert and S. W. Glunz, *Energy Environ. Sci.*, 2024, **17**, 1781–1818.
13 T. Kirchartz, G. H. Yan, Y. Yuan, B. K. Patel, D. Cahen and P. K. Nayak, *Nat. Rev. Mater.*, 2025, **10**, 335–354.
14 D. P. McMeekin, P. Holzhey, S. O. Fünrer, S. P. Harvey, L. T. Schelhas, J. M. Ball, S. Mahesh, S. Seo, N. Hawkins, J. F. Lu, M. B. Johnston, J. J. Berry, U. Bach and H. J. Snaith, *Nat. Mater.*, 2023, **22**, 73–83.
15 X. Chen, W. Hui, Q. Wang, P. Xu, Z. L. Xu, B. Fan, L. Song, X. P. Xu, Y. H. Wu and Q. Peng, *Nat. Commun.*, 2025, **16**, 9717.
16 J. J. Zhou, Y. X. Luo, R. D. Li, L. W. Tian, K. Zhao, J. H. Shen, D. E. Jin, Z. X. Peng, L. B. Yao, L. Zhang, Q. Q. Liu, S. C. Zhang, L. Jin, S. L. Chu, S. S. Wang, Y. Tian, J. Z. Xu, X. Zhang, P. J. Shi, X. A. Wang, W. Fan, X. C. Sun, J. Y. Sun, L. Z. Chen, G. Wu, W. Shi, H. F. Wang, T. Q. Deng, R. Wang, D. R. Yang and J. J. Xue, *Nat. Chem.*, 2025, **17**, 564–570.
17 X. N. Sun, X. Wang, J. P. Zhang, P. Xu, W. Zhang, Z. H. Zhang, W. D. Shi, T. J. Liu and X. M. Zhao, *ACS Energy Lett.*, 2025, **10**, 5356–5362.
18 Y. B. Yuan and J. S. Huang, *Acc. Chem. Res.*, 2016, **49**, 286–293.
19 W. K. Zhu, S. R. Wang, X. Zhang, A. L. Wang, C. Wu and F. Hao, *Small*, 2022, **18**, 2105783.
20 Z. C. Shen, Q. F. Han, X. H. Luo, Y. Z. Shen, Y. B. Wang, Y. B. Yuan, Y. Q. Zhang, Y. Yang and L. Y. Han, *Nat. Photonics*, 2024, **18**, 450–457.
21 J. M. Azpiroz, E. Mosconi, J. Bisquert and F. De Angelis, *Energy Environ. Sci.*, 2015, **8**, 2118–2127.
22 C. Eames, J. M. Frost, P. R. F. Barnes, B. C. O'Regan, A. Walsh and M. S. Islam, *Nat. Commun.*, 2015, **6**, 7497.
23 S. Meloni, T. Moehl, W. Tress, M. Franckevicius, M. Saliba, Y. H. Lee, P. Gao, M. K. Nazeeruddin, S. M. Zakeeruddin, U. Rothlisberger and M. Graetzel, *Nat. Commun.*, 2016, **7**, 10334.
24 O. S. Game, G. J. Buchsbaum, Y. Y. Zhou, N. P. Padture and A. I. Kingon, *Adv. Funct. Mater.*, 2017, **27**, 1606584.
25 M. H. Futscher, J. M. Lee, L. McGovern, L. A. Muscarella, T. Y. Wang, M. I. Haider, A. Fakharuddin, L. Schmidt-Mende and B. Ehrler, *Mater. Horiz.*, 2019, **6**, 1497–1503.
26 M. H. Futscher, M. K. Gangishetty, D. N. Congreve and B. Ehrler, *J. Chem. Phys.*, 2020, **152**, 044202.
27 S. Reichert, J. Flemming, Q. Z. An, Y. Vaynzof, J. F. Pietschmann and C. Deibel, *Phys. Rev. Appl.*, 2020, **13**, 034018.
28 L. McGovern, M. H. Futscher, L. A. Muscarella and B. Ehrler, *J. Phys. Chem. Lett.*, 2020, **11**, 7127–7132.
29 L. McGovern, G. Grimaldi, M. H. Futscher, E. M. Hutter, L. A. Muscarella, M. C. Schmidt and B. Ehrler, *ACS Appl. Energy Mater.*, 2021, **4**, 13431–13437.
30 X. L. Wang, Z. Y. Jiao, H. H. Fang, J. Zhan, D. D. Cao, X. Huang, Y. Wang, X. C. Ai and J. P. Zhang, *Nano Lett.*, 2024, **24**, 16443–16449.
31 T. Zhang, H. N. Chen, Y. Bai, S. Xiao, L. Zhu, C. Hu, Q. Z. Xue and S. H. Yang, *Nano Energy*, 2016, **26**, 620–630.
32 R. García-Rodríguez, D. Ferdani, S. Pering, P. J. Baker and P. J. Cameron, *J. Mater. Chem. A*, 2019, **7**, 22604–22614.
33 D. J. Xue, Y. Hou, S. C. Liu, M. Y. Wei, B. Chen, Z. R. Huang, Z. B. Li, B. Sun, A. H. Proppe, Y. T. Dong, M. I. Saidaminov, S. O. Kelley, J. S. Hu and E. H. Sargent, *Nat. Commun.*, 2020, **11**, 1514.
34 S. Tan, I. Yavuz, N. De Marco, T. Y. Huang, S. J. Lee, C. S. Choi, M. H. Wang, S. Nuryyeva, R. Wang, Y. P. Zhao, H. C. Wang, T. H. Han, B. Dunn, Y. Huang, J. W. Lee and Y. Yang, *Adv. Mater.*, 2020, **32**, 1906995.
35 Z. Y. Ni, H. Y. Jiao, C. B. Fei, H. Y. Gu, S. Xu, Z. H. Yu, G. Yang, Y. A. Deng, Q. Jiang, Y. Liu, Y. F. Yan and J. S. Huang, *Nat. Energy*, 2022, **7**, 65–73.
36 L. A. Muscarella, E. M. Hutter, F. Wittmann, Y. W. Woo, Y. K. Jung, L. McGovern, J. Versluis, A. Walsh, H. J. Bakker and B. Ehrler, *ACS Energy Lett.*, 2020, **5**, 3152–3158.
37 S. Reichert, Q. Z. An, Y. W. Woo, A. Walsh, Y. Vaynzof and C. Deibel, *Nat. Commun.*, 2020, **11**, 6098.
38 B. A. Li, C. X. Kan, P. J. Hang, Y. J. Fang, L. J. Zuo, L. H. Song, Y. Q. Zhang, D. R. Yang and X. G. Yu, *Phys. Status Solidi RRL*, 2021, **15**, 2100225.
39 N. Liu and C. Y. Yam, *Phys. Chem. Chem. Phys.*, 2018, **20**, 6800–6804.
40 A. Mishra, M. A. Hope and L. Emsley, *ACS Energy Lett.*, 2024, **9**, 5074–5080.
41 K. L. Svane, A. C. Forse, C. P. Grey, G. Kieslich, A. K. Cheetham, A. Walsh and K. T. Butle, *J. Phys. Chem. Lett.*, 2017, **8**, 6154–6159.

42 T. Y. Huang, S. Tan, S. Nuryyeva, I. Yavuz, F. Babbe, Y. Zhao, M. Abdelsamie, M. H. Weber, R. Wang, K. N. Houk, C. M. Sutter-Fella and Y. Yang, *Sci. Adv.*, 2021, **7**, abj1799.
43 C. G. Bischak, C. L. Hetherington, H. Wu, S. Aloni, D. F. Ogletree, D. T. Limmer and N. S. Ginsberg, *Nano Lett.*, 2017, **17**, 1028–1033.
44 Y. C. Zhao, W. K. Zhou, X. Zhou, K. H. Liu, D. P. Yu and Q. Zhao, *Light: Sci. Appl.*, 2017, **6**, e16243.
45 E. T. Hoke, D. J. Slotcavage, E. R. Dohner, A. R. Bowring, H. I. Karunadasa and M. D. McGehee, *Chem. Sci.*, 2015, **6**, 613–617.
46 D. Meggiolaro, E. Mosconi and F. De Angelis, *ACS Energy Lett.*, 2019, **4**, 779–785.